

Analytical Models for Determining the Propagation of Rectangular Surface Jets for Fishway Attraction Flow

Veronica Wiering¹, Patrick Heneka², Martin Henning³, Linda Bergmann⁴

Abstract

The present paper evaluates suitability of two analytical models to determine the propagation of rectangular surface jets as a tool to design fishway attraction flow. It focuses on rectangular orifices of vertical slot fishways with aspect ratios (width-to-height) for $W/H < 1$. Both models were rewritten to match boundary conditions for fishways because they were initially derived for horizontal orifices. As the basis for the evaluation, the output of the analytical models to RANS simulations for 12 geometries $1/16 \leq W/H \leq 4$ is compared. Applied analytical equations for half-lengths for cases $W/H \geq 1/4$ are within 5% of RANS modeling results for all cases. The location of centerline transition locations from analytical models also agree reasonably well with RANS modeling. The findings support efficient design of optimum attraction flow propagation using simple, rapid analytical approaches.

Keywords

RANS; three-dimensional jet; centerline velocity decay; half-length; fish passage design

¹veronica.wiering@baw.de, Federal Waterways Engineering and Research Institute (BAW), Karlsruhe, Germany

²patrick.heneka@baw.de, Federal Waterways Engineering and Research Institute (BAW), Karlsruhe, Germany


³martin.henning@baw.de, Federal Waterways Engineering and Research Institute (BAW), Karlsruhe, Germany

⁴l.bergmann@ghj.de, GHJ, Karlsruhe, Germany

This paper was submitted on 8 July 2021. It was accepted after double-blind review on 24 February 2022 and published online on 11 April 2022.

DOI: <https://doi.org/10.48438/jchs.2022.0011>

Cite as: "Wiering, V., Heneka, P., Henning, M. & Bergmann, L. Analytical Models for Determining the Propagation of Rectangular Surface Jets for Fishway Attraction Flow. Journal of Coastal and Hydraulic Structures, 2. <https://doi.org/10.48438/jchs.2022.0011>"

The Journal of Coastal and Hydraulic Structures is a community-based, free, and open access journal for the dissemination of high-quality knowledge on the engineering science of coastal and hydraulic structures. This paper has been written and reviewed with care. However, the authors and the journal do not accept any liability which might arise from use of its contents. Copyright ©2021 by the authors. This journal paper is published under a CC-BY-4.0 license, which allows anyone to redistribute, mix and adapt, as long as credit is given to the authors. 

1 Introduction

Creation of an optimum attraction flow is critical for fishes to efficiently locate and volitionally enter fishway entrances (e.g. Larinier 1992; Castro-Santos and Haro 2010). An ideal fishway attraction flow must be of sufficient discharge and shape to create an uninterrupted migratory corridor perceptible by fishes downstream of a barrier (e.g. Williams et al. 2012). Determination of attraction flow propagation must consider site-specific hydraulic and solid boundary conditions and the behavior of target fishes (Heneka et al. 2021). Inhomogeneous and turbulent flow associated with the fishway entrance pool and vertical slot, and also bank near reversed flow and turbulent turbine discharge will reduce the attraction flow length, whereas solid boundaries near the entrance slot may enhance attraction flow lengths

because of the coanda effect (e.g. Mahl et al. 2021). Results of detailed numerical hydrodynamic or physical scale model investigations may be applied in the planning process to assess attraction flow propagation patterns of projected fishways (Gisen et al 2017; Kopecki et al. 2014). However, these methods are time- and cost-intensive. Cost and schedule demands for the large number of fishways required for German dams limit the routine use of sophisticated hydraulic modeling studies to a few specific cases that are of interest for scientific or other purposes. On this understanding, treating attraction flow from a rectangular fishway entrance as a turbulent surface jet may provide efficient tools to simplify propagation length and shape estimates.

Jets occur in many fluid processes (e.g. in wastewater treatment or aviation) where their mixing characteristics are well researched. Jet characteristics mainly depend on orifice geometry, outlet velocity, Reynolds number, and ambient fluid properties (Kraatz 1975; Rajaratnam 1976; Tsuchiya et al. 1986; Walker 1997; Quinn 2006). Depending on boundary conditions, a distinction is made between free jets, which are completely submerged, and surface and wall jets, which attach to the water surface or solid boundaries, respectively. Jets may be further classified into axisymmetric (i.e., round), two-dimensional (i.e., plane), or three-dimensional (i.e., rectangular), depending on orifice geometry.

The aspect ratio of the orifice W/H (width-to-height) is a determining factor for jet propagation lengths for rectangular orifices (Rajaratnam 1976; Marsters and Fortheringham 1980; Quinn 1992; Seo and Kwon 2005). W/H for fishway entrance slots vary over time because while widths are commonly fixed, entrance water depths change as tailwater levels change. Entrance slot widths for German waterways are usually between 0.4 m and 1.5 m and water depths during operation of the fishway range between 1 m and 4 m.

Based on the above, fishway attraction flows may be treated as rectangular surface jets for W/H ranges between 1/8 and 1. Systematic research on rectangular jet propagation is only validated for $W/H > 1$ with a focus on free jets (Krothapalli et al. 1981; Rajaratnam and Humphries 1984; Seo and Kwon 2005). Rectangular free jets with $W/H > 1$ show three distinct decay regions along the longitudinal centerline x (Figure 1):

- i) A tapered core zone directly downstream of the orifice for $0 < x < x_1$, in which the fluid's centerline velocity is equal to the outlet velocity (Kraatz 1975; Rajaratnam 1976).
- ii) An adjacent two-dimensional zone for $x_1 < x < x_2$ where centerline velocities decrease proportionally with $x^{-1/2}$ due to mixing with the ambient fluid. Downstream of x_1 , centerline velocity profiles for the shorter vertical axis (minor axis) are self-similar in the streamwise direction (Sforza et al. 1966; Marsters and Fortheringham 1980), but profiles for the longer horizontal axis (major axis) are still in transition to the axisymmetric zone (Demissie 1980; Marsters and Fortheringham 1980; Krothapalli et al. 1981; Quinn 1992; Seo and Kwon 2005).
- iii) An axisymmetric zone for $x > x_2$, where velocity profiles of both axes are self-similar in streamwise direction and the centerline velocity decay is proportional with x^{-1} (Demissie 1980; Seo and Kwon 2005).

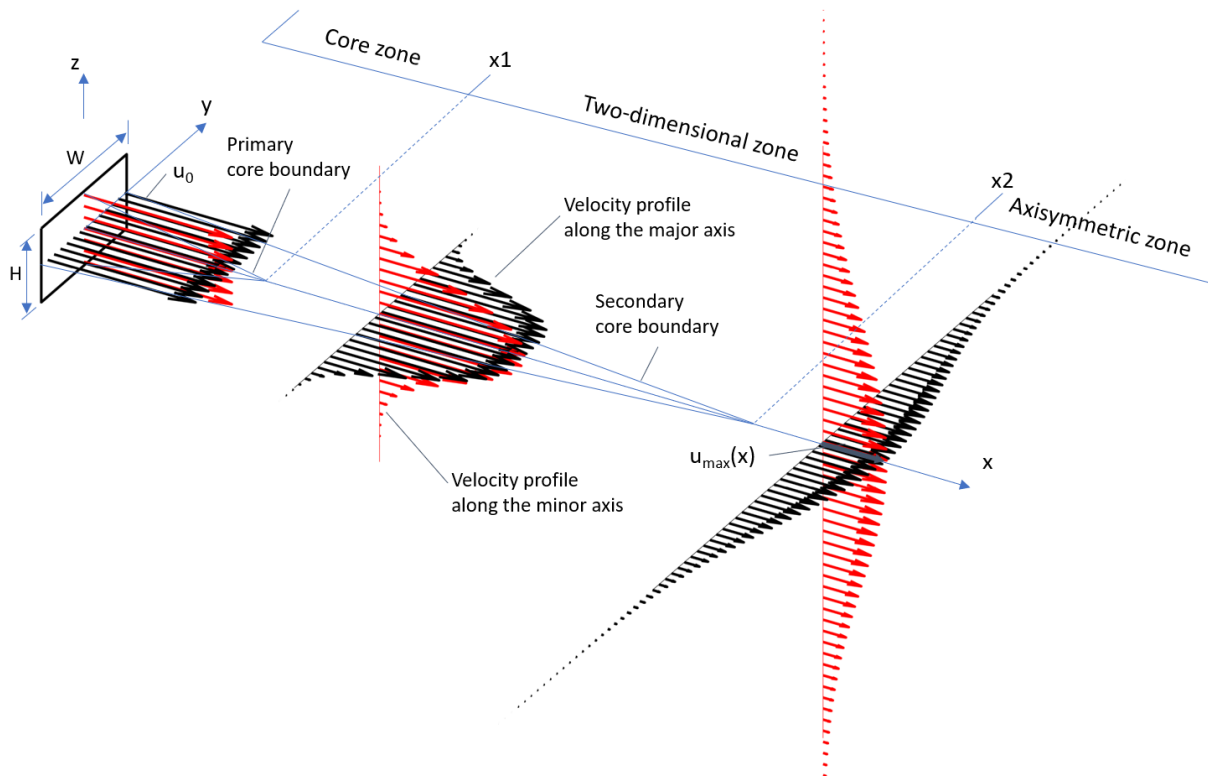


Figure 1: Schematic of a rectangular free jet with $W/H = 2$ where: x denotes the longitudinal centerline and y and z are lateral and vertical axes, respectively; $x = 0$ denotes the outlet plane; x_1 marks the transition between the core and two-dimensional zones; x_2 marks the transition between two-dimensional and axisymmetric zones; u_0 is the outlet velocity and $u_{max}(x)$ is the maximum velocity at the centerline.

The downstream extension of the different decay regions depends on W/H (Sforza et al. 1966; Marsters and Fortheringham 1980; Krothapalli et al. 1981; Quinn 1992; Seo and Kwon 2005). The two-dimensional zone extends further downstream as W/H increasingly deviates from 1. For rectangular jets with $W/H > 1$, the transition location from the two-dimensional zone to the axisymmetric zone x_2 depends on W (Krothapalli et al. 1981; Seo and Kwon 2005). For square orifices $W/H = 1$, the two-dimensional zone is displaced by the axisymmetric zone and, as a result, only the core and axisymmetric zones exist (Seo and Kwon 2005).

For plane and round free jets only two zones exist: the core zone $x < x_1$ and either the two-dimensional zone for plane jets or the axisymmetric zone for round jets. The velocity decay rate for $x < x_1$ is proportional to $x^{-1/2}$ and x^{-1} for plane and round jets, respectively (Kraatz 1975; Rajaratnam and Humphries 1984). Velocity profiles are characterized by self-similarity of different cross-sections in the streamwise direction (Kraatz 1975; Rajaratnam 1976).

Surface jets differ from free jets because their vertical propagation is bounded by the water surface, where a surface current, characterized by higher lateral velocities, occurs. Below the surface current, surface jets exhibit self-similarity in the same way as free jets, which leads to the same characteristic decay regions (Madnia and Bernal 1994; Walker 1997; Gholamreza-Kashi et al. 2007).

The present study aims at closing the knowledge gap that exists for assessing propagation of rectangular surface jets emergent from typical vertical slot fishways. In this, analytical models established for rectangular horizontal free jets with $W/H > 1$ (Demissie 1980) and for plane and round free jets (Kraatz 1975) are extended and validated under homogeneous boundary conditions for rectangular surface jets with $W/H < 1$. In doing so, the analytical models are compared with three-dimensional RANS modelling for seven different aspect ratios $1/16 \leq W/H \leq 4$ and results of studies of free and surface jets available in the scientific literature.

2 Analytical Models

2.1 General remarks

Downstream evolution of centerline velocities may be used as the primary metric to describe propagation of rectangular surface jets for $W/H < 1$ and $W/H > 1$ (Figure 2). Velocity distribution at the orifice is assumed homogeneous with an average bulk velocity u_0 . Surface currents are omitted as they solely affect local velocities in a small surface layer (Walker 1997; Gholamreza-Kashi et al. 2007). Using the water surface as symmetry plane, surface jets may be defined as half-free jets. Consequently, effective jet height H equals two times the actual water depth h at the orifice as $H = 2h$. Shorter and longer axis of the rectangular orifice are denoted as minor and major axis, respectively. Hence, the assignment of W and H as minor and major axis depends on W/H and reverses at $W/H = 1$.

The general pattern of jet propagation in the absence of solid boundary effects is described as follows (Figure 2):

- 1) velocities in the core zone equal u_0 and delimit the core zone from the two dimensional and axisymmetric zones where velocity decays,
- 2) maximum velocities at each profile $u_{max}(x)$ occur along the x-axis centerline (at $y = 0, z = 0$),
- 3) $x_1 < x < x_2$ velocities in the plane of the minor axis with x are self-similar,
- 4) $x > x_2$ velocities are self-similar in all planes,
- 5) core zone length x_1 depends on the dimension of the minor axis, whereas the dimension of the major axis determines x_2 , and
- 6) scale of the three decay regions depends on orifice aspect ratio.

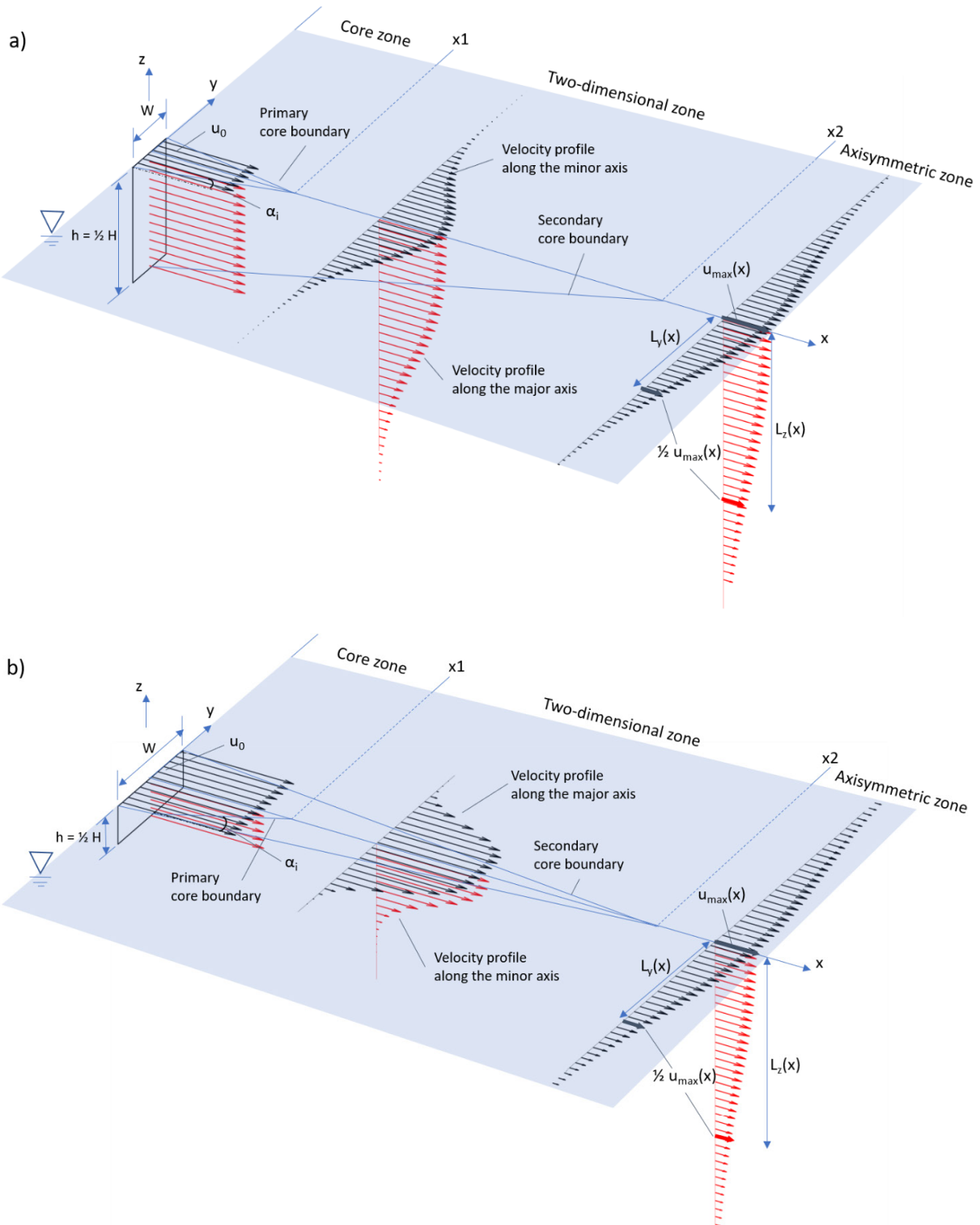


Figure 2: Schematics of rectangular surface jets for (a) vertical orifice $W/H < 1$ and (b) horizontal orifice $W/H > 1$. α_i denotes the inner diffusion angle (see chapter 2.3).

L_x , $L_y(x)$ and $L_z(x)$ are used to unambiguously define the spatial extent of the jet to identify the influence of different W/H ratios on jet propagation. Longitudinal jet propagation is described using centerline velocity decay rate $u_{max}(x)/u_0$ where jet half-length L_x is

$$\frac{u_{max}(L_x)}{u_0} = 0.5 \tag{1}$$

Lateral $L_y(x)$ and vertical $L_z(x)$ propagation half-widths are

$$\frac{u(L_y(x))}{u_{max}(x)} = 0.5 \quad \text{for } x > x_1 \quad (2)$$

$$\frac{u(L_z(x))}{u_{max}(x)} = 0.5 \quad \text{for } x > x_1 \quad (3)$$

Note, that $L_y(x)$ equals $L_z(x)$ for $x > x_2$.

2.2 Point Source Concept (PSC)

Demissie (1980) uses Reichardt's hypothesis (1943) to linearize the momentum equation in the direction of flow for a steady, incompressible, and free turbulent flow. Using the Point Source Concept (PSC), where the discharge area of a rectangular slot jet is subdivided into small, individual sources, it is possible to superimpose the particular solutions of each point source and finally to obtain relationships describing velocity decay. The concept has been validated for horizontal orifices ($W/H > 1$).

Using PSC, the time-averaged velocity field of free jets (in Demissie (1980), they are called deeply submerged jets) is described with the error function (erf) by

$$\frac{\overline{u^2}}{(\overline{u^2})_0} = \frac{1}{4} \left[\operatorname{erf}\left(\frac{W+2y}{2cx}\right) + \operatorname{erf}\left(\frac{W-2y}{2cx}\right) \right] \times \left[\operatorname{erf}\left(\frac{H+2z}{2cx}\right) + \operatorname{erf}\left(\frac{H-2z}{2cx}\right) \right] \quad (4)$$

where c denotes the spreading coefficient of the jet which is an unknown to be determined from experimental data. As proposed by Demissie (1980) for long channel outlet geometries $c = 0.087$ is used. The origin of the coordinate system is in the center of the rectangular outlet.

Considering symmetry at $z = 0$, eq. (4) can be rewritten for surface jets by using an effective jet height $h = H/2$ resulting in $W/h = 2W/H$. The velocity decay at the centerline ($y = z = 0$) may be written as

$$\frac{u_{max}(x)}{u_0} = \left[\operatorname{erf}\left(\frac{1}{2cx/W}\right) \times \operatorname{erf}\left(\frac{1}{2W/Hcx/W}\right) \right]^{\frac{1}{2}} \quad (5)$$

2.3 Inner Diffusion Angle Concept (IDAC)

Kraatz (1975) introduced the inner diffusion angle α_i (Figure 2), which is affected by initial turbulence at the orifice (Kraatz 1975; Kümmel 2004). It is a measure of the mixing processes of a free turbulent jet with the ambient fluid that drive the expansion of the zones. Based on Kraatz's centerline velocity equations for plane and round free jets equations for the longitudinal evolution of centerline velocities for rectangular surface jets with arbitrary aspect ratios are derived. This method is denoted as the Inner Diffusion Angle Concept (IDAC) and dimensionless equations for transition locations x_1 and x_2 as a function of W , H and α_i for $W/H < 1$ are proposed as:

$$\frac{x_1}{W} = \frac{1}{2 \tan(\alpha_i)} \quad (6)$$

$$\frac{x_2}{W} = \frac{1}{2W/H \tan(\alpha_i)} \quad (7)$$

For $W/H > 1$ the transition locations x_1 and x_2 switch because the minor and major axes switch. The inner diffusion angle α_i is set to 5.0° which is the midpoint of the reported range of 4.5° to 5.5° (Kraatz 1975). For surface jets, Kraatz (1975) also derives an equation for transition locations x_2 for $W/H > 1$ (which agrees with eq. (7)) using experimental

data from Wiegel et al. (1965). Based on eqs. (6) and (7), the centerline velocity in the three distinct decay regions can be calculated. Independent of W/H the centerline velocity in the core zone is

$$\frac{u_{max}(x)}{u_0} = 1 \quad \text{for } x < x_1. \quad (8)$$

Analytical approaches also apply to the two-dimensional and axisymmetric zones. In the two-dimensional zone $x_1 < x < x_2$ the jet shows the characteristics of a plane jet with decay rate $u \sim x^{-1/2}$ (Kraatz 1975; Rajaratnam and Humphries 1984). Centerline velocities for $W/H < 1$ and $W/H > 1$ for $x_1 < x < x_2$ are calculated by

$$\frac{u_{max}(x)}{u_0} = \frac{1}{\sqrt{2 \tan(\alpha_i)}} \frac{1}{\sqrt{x/W}} \quad W/H < 1 \quad (9)$$

$$\frac{u_{max}(x)}{u_0} = \frac{1}{\sqrt{2 W/H \tan(\alpha_i)}} \frac{1}{\sqrt{x/W}} \quad W/H > 1 \quad (10)$$

In the axisymmetric zone $x > x_2$ centerline velocity decay is identical to that of a round jet with decay rate of $u \sim x^{-1}$ (Kraatz 1975; Rajaratnam and Humphries 1984). Centerline velocities for all W/H are calculated by

$$\frac{u_{max}(x)}{u_0} = \frac{1}{\sqrt{W/H} 2 \tan(\alpha_i)} \frac{1}{x/W} \quad \text{for } x > x_2. \quad (11)$$

Decay of centerline velocity can be summarized in relative distance x/W across the different jet zones for $0 \leq W/H \leq 5$ using eqs. (8) – (11) (Figure 3). In general, the axisymmetric zone extent decreases and occurs further downstream when W/H decreases for $W/H < 1$ (eq. (9)) or increases for $W/H > 1$ (eq. (10)). With decreasing axisymmetric zone, the two-dimensional zone extends accordingly further into the tailwater. At $W/H = 1$ only core and axisymmetric zone occur.

Adding different centerline velocity ratios $u_{max}(x)/u_0$ (Figure 3), transition locations x_2/W for $W/H = 1/2$ and $W/H = 2$ or $W/H = 1/4$ and $W/H = 4$ show that x_2/W occurs at the same $u_{max}(x)/u_0$ -ratio in each case. It follows, that the transition locations x_2/W are proportional with x^{-1} .

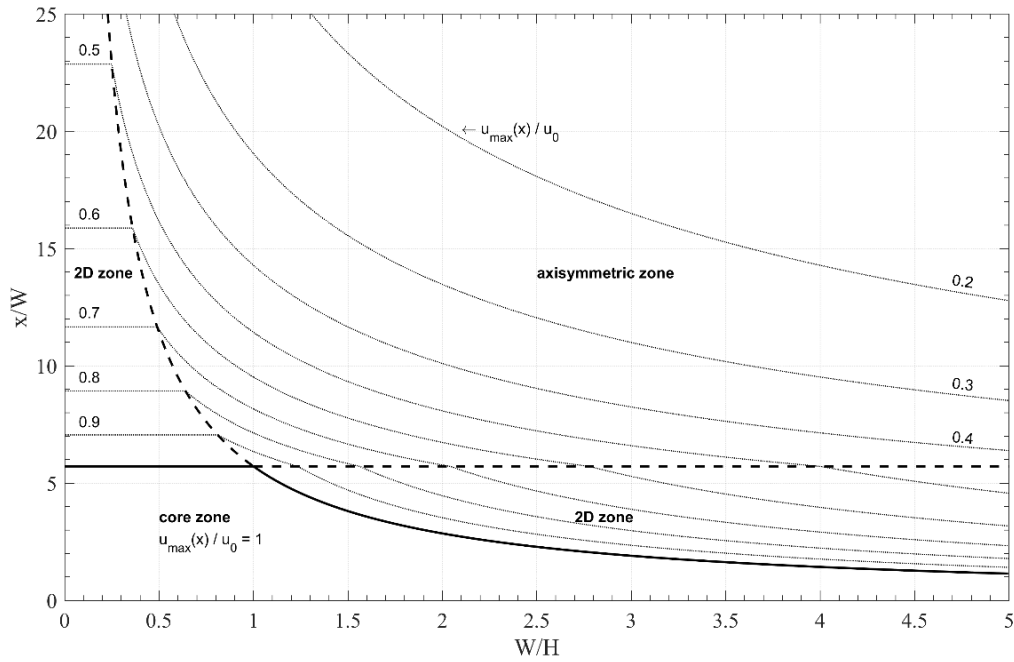


Figure 3: Characteristic decay regions for surface jets with different W/H and centerline velocity ratios $u_{max}(x)/u_0$ for $\alpha_i = 5^\circ$ for turbulent rectangular surface jets. Bold lines mark the transition location x_1 ; dashed lines mark the transition location x_2 .

The minor vertical half-width $L_z(x)/W$ for a three-dimensional rectangular jet with $W/H > 1$ or $L_y(x)/W$ for $W/H < 1$ must be estimated because the concept of Kraatz (1975) was developed only for plane (i.e., two-dimensional) free jets:

$$\frac{L_z(x)}{W} = C \left(\frac{x}{W} + \frac{x_0}{W} \right) \quad W/H > 1 \quad (12)$$

$$\frac{L_y(x)}{W} = C \left(\frac{x}{W} + \frac{x_0}{W} \right) \quad W/H < 1 \quad (13)$$

where C is a spreading coefficient and x_0 is the distance from the orifice to a hypothetical virtual origin. Values for x_0 vary and can be positive or negative depending on different initial conditions and turbulent levels at the orifice (Krothapalli et al. 1981) and are influenced by the maximum measured axial distance (Seo and Kwon 2005).

3 Numerical Model

The performance of the two analytical models described previously is assessed and estimates of centerline velocity decay, jet half-lengths and half-widths are compared with the solutions obtained from three-dimensional Reynolds-averaged-Navier-Stokes (RANS) modeling for different aspect ratios. The governing equations for the conservation of mass and momentum for an incompressible, steady, three-dimensional flow in Cartesian tensor notation using Einstein summation convention are

$$\frac{\partial \bar{u}_i}{\partial x_i} = 0 \quad (14)$$

$$\bar{u}_j \frac{\partial(\rho \bar{u}_i)}{\partial x_i} = -\frac{\partial \bar{p}}{\partial x_i} + \frac{\partial}{\partial x_j} \left(\mu \rho \frac{\partial \bar{u}_i}{\partial x_j} - \rho \overline{u'_i u'_j} \right) \quad (15)$$

where \bar{p} = mean fluid pressure, μ = dynamic viscosity of water, \bar{u}_i = mean velocity components and ρ = water density. Mean flow eqs. (14) and (15) were solved using the finite volume simpleFoam solver (OpenFOAM version 2.3.1 (Weller et al. 1998)) using the Semi-Implicit Method for Pressure-Linked Equations (Patankar 1980). For the unknown Reynolds stresses $\overline{u'_i u'_j}$, the k- ω SST model is used as implemented in OpenFOAM version 2.3.1 (Menter and Esch 2001; Menter et al. 2003) as it combines the advantages of the k- ω and k- ϵ model by using k- ω near the wall and k- ϵ in the free flow region (Rodi 2017). The basic equations for the kinetic turbulence energy k and the turbulence dissipation rate ω are

$$\frac{\partial(\rho k)}{\partial t} + \frac{\partial(\rho \bar{u}_j k)}{\partial x_j} = \tilde{P}_k - \beta^* \rho k \omega + \frac{\partial}{\partial x_j} \left[(\mu + \sigma_{k1} \mu_t) \frac{\partial k}{\partial x_j} \right] \quad (16)$$

$$\frac{\partial(\rho \omega)}{\partial t} + \frac{\partial(\rho \bar{u}_j \omega)}{\partial x_j} = \alpha \rho S^2 - \beta \rho \omega^2 + \frac{\partial}{\partial x_j} \left[(\mu + \sigma_\omega \mu_t) \frac{\partial \omega}{\partial x_j} \right] + 2(1 - F_1) \rho \sigma_{\omega 2} \frac{1}{\omega} \frac{\partial k}{\partial x_i} \frac{\partial \omega}{\partial x_i} \quad (17)$$

where F_1 is a blending function for switching between the k- ω and k- ϵ formulation, \tilde{P}_k is a production limiter of turbulence in stagnation regions, S is the invariant measure of the strain rate, and μ_t is the turbulent eddy viscosity. All constants are computed by blending the corresponding constants (e.g. $\alpha = \alpha_1 F_1 + \alpha_2 (1 - F_1)$). The constants used for computation are $\beta^* = 0.09$, $\sigma_{k1} = 0.85$, $\alpha_1 = 5/9$, $\beta_1 = 0.075$, $\sigma_{w1} = 0.5$, $\alpha_2 = 0.44$, $\beta_2 = 0.0828$, $\sigma_{k2} = 1$ and $\sigma_{\omega 2} = 0.856$ (Menter et al. 2003).

The model domain consists of a cubic waterbody and a rectangular inlet with different aspect ratios represented in a Cartesian coordinate system (Figure 1). The model domain spans 40 m in the x- and y-directions and 20 m in the z-direction. Computational meshes are generated using the blockMesh tool implemented in OpenFOAM. Each configuration required a unique interchangeable assigned mesh describing a specific inlet size with local refinements in regions with strong gradients (e.g. around the jet core). The cell sizes are 0.05 m in the jet and increase to the boundaries.

The water surface (x-y plane at $z = 0$) is modeled as a slip boundary for velocity with zero normal gradient for p , k and ω . The inlet turbulence kinetic energy and its specific turbulent dissipation are calculated as

$$k_{in} = 1.5 I u_0^2 \quad (18)$$

$$\omega_{in} = \frac{k_{in}^{0.5}}{C_\mu^{0.25} L} \quad (19)$$

with $C_\mu^{0.25} = 0.09$. The inlet turbulence intensity $I = 0.16$ and the turbulent mixing length $L = 1.21 \cdot 10^{-3} m$ are set based on preliminary testing. The flow velocity at the inlet is set to a uniform profile of $u_0 = 1.5 m/s$ by a Dirichlet boundary condition and a fixed pressure is set at the outlet. A zero gradient was set along the axial direction for u , k and ω . Walls and bottom have slip boundary conditions for velocity and zero gradient conditions for p , k , ω .

Table 1 lists the parameters of the RANS simulations. Inlet aspect ratios W/H varied from 1/16 to 4. Reynolds and Froude number are based on the hydraulic diameter with

$$4R_{hy} = \frac{Wh}{W + 2h} \quad (20)$$

and kinematic viscosity is assumed to be $1 \cdot 10^{-6} m^2/s$. Simulations were initialized to zero except at the boundaries. Solutions were considered convergent when the maximum residual of all the discretized equations was below 10^{-5} .

Table 1: Parameters of the RANS simulations.

No.	W/H [-]	W [m]	h [m]	4 R _{hy} [m]	Re [10 ⁶]	Fr [-]
1	1/16	0.5	4.0	0.94	1.41	0.49
2	1/8	0.5	2.0	0.89	1.33	0.51
3	1/4	0.5	1.0	0.80	1.20	0.54
4	1/4	1.0	2.0	1.60	2.40	0.38
5	1/2	0.5	0.5	0.67	1.00	0.59
6	1/2	1.0	1.0	1.33	2.00	0.42
7	1/2	2.0	2.0	2.67	4.00	0.29
8	1.0	1.0	0.5	1.00	1.50	0.48
9	1.0	2.0	1.0	2.00	3.00	0.34
10	2.0	2.0	0.5	1.33	2.00	0.42
11	2.0	4.0	1.0	2.67	4.00	0.29
12	4.0	4.0	0.5	1.60	2.40	0.38

3.1 Model validation

The numerical model was validated by comparing its temporal mean velocity profiles in lateral and longitudinal directions to the experimental data of Gholamreza-Kashi et al. (2007). Their data were obtained for a turbulent rectangular surface jet with an aspect ratio of $W/H = 1$, an inlet jet profile produced by a convergent orifice, and a Reynolds number of 8,850 (based on the hydraulic diameter).

The longitudinal evolution of the normalized centerline velocity component $u_{max}(x)/u_0$ against x/W from the simulation shows good agreement to experimental data (Figure 4a). The lateral distribution of normalized streamwise velocity components $u/u_{max}(x)$ in the axisymmetric zone for $y/L_y(x)$ for three discrete x/W correspond to a single-sided normalized velocity profile for the x-y plane (Figure 4b). RANS results show good agreement with experimental data of Gholamreza-Kashi et al. (2007) with a slight overestimation of velocities $u/u_{max}(x) < 0.4$. Notably, centerline velocities u are less than 0.01 m/s for $y/L_y(x) < -2$.

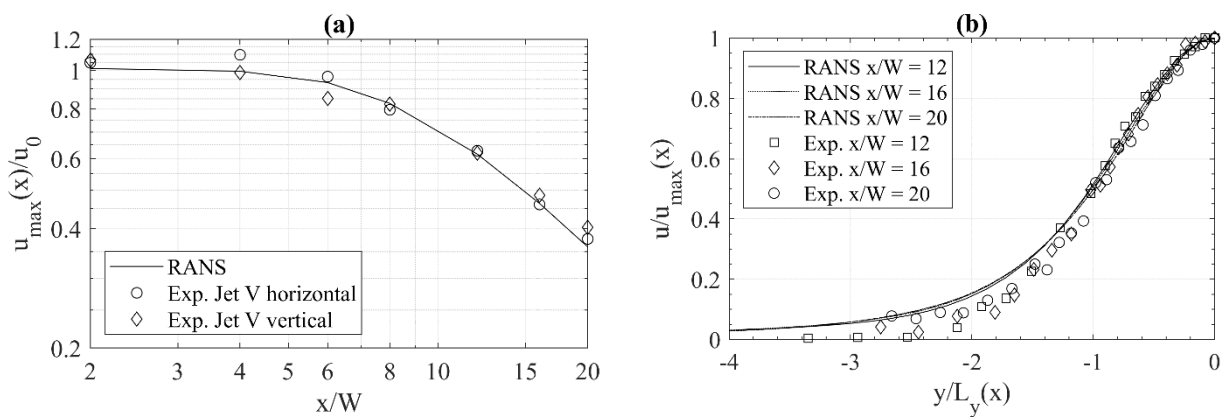


Figure 4: (a) Longitudinal distribution of the maximum centerline velocity, (b) horizontal profile of the centerline velocity component below the surface ($z = L_z$) at $Re = 8,850$. Experimental measurements (denoted as Exp.) are from Gholamreza-Kashi et al. (2007).

4 Results

4.1 Flow Fields

The longitudinal and lateral jet propagation results from RANS modeling are compared with results from the PSC (eq. ((4))) using isoline plots at the water surface for $W/H = 1/8$ and $W/H = 1/2$ (Figure 5). Results for IDAC are not displayed because it only provides equations for centerline velocity decay. Both lateral and centerline velocities decrease as the jet spreads laterally and loses momentum to the ambient fluid. The transition between core and two-dimensional zones appears at $x_1/W = 5$ and $x_1/W = 4$ for RANS simulations of $W/H = 1/8$ and $W/H = 1/2$, respectively, indicating velocities decay slower and jet propagation is longer for $W/H = 1/8$. Consequently, L_x (eq. ((1))) extends further downstream for $W/H = 1/8$ (at $x/W = 26$) than for $W/H = 1/2$ ($x/W = 17$) (not shown in the figure). Propagation length along the centerline is longer for the PSC simulation for $W/H = 1/8$ than for the RANS results. At $x/W \geq 12$ the velocity decay for the RANS modeling and PSC agree (not shown in the figure). In contrast, for $W/H = 1/2$ the centerline velocity decay is faster for PSC results. The deviation in the y-propagation at $x/W = 15$ about -15% for $W/H = 1/8$ and about $+5\%$ for $W/H = 1/2$.

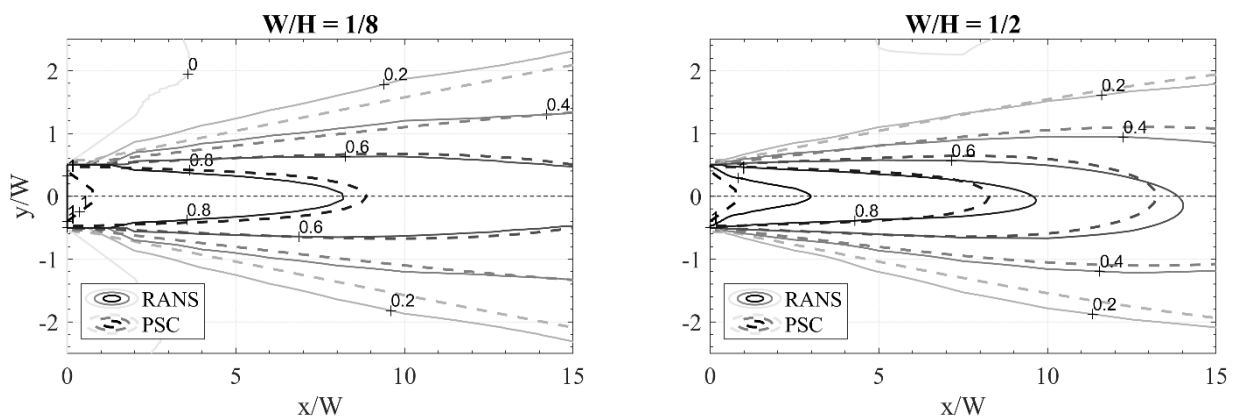


Figure 5: 2D-Flow field at the water surface ($z = 0$) for W/H of $1/8$ and $1/2$ according to RANS simulations 2 and 7 (Table 1) and PSC.

4.2 Centerline Velocity Decay

The downstream propagation of normalized centerline velocities at the water surface ($y = 0, z = 0$) was evaluated for all aspect ratios W/H obtained from RANS simulations and compared to predictions using PSC and IDAC equations (Figure 6). Velocities are normalized with the bulk mean and plotted against the relative longitudinal distance from the orifice exit section. Multiple velocity values are obtained from multiple RANS simulations performed for the same aspect ratio for $1/4 \leq W/H \leq 2$. However, by normalizing x with W the streamwise expansion of the displayed results differs.

Centerline velocities predicted with PSC qualitatively agree with RANS results for all simulations. Maximum deviations of $u_{max}(x)/u_0$ in the core zone $x < x_1$ and two-dimensional zone $x < x_2$ are between -4% and $+4\%$ with positive deviations for small aspect ratios $W/H < 1$ and negative deviations for $W/H > 1$. In the axisymmetric zone, velocities are overestimated by 3% at $u_{max}(x)/u_0 = 0.3$ for all aspect ratios. Both RANS and PSC predict smooth transitions between zones.

Centerline velocities predicted with IDAC are discontinuous and distinct transition locations are clearly identifiable. As a result, $u_{max}(x)/u_0$ at the transition between core zone and two-dimensional zone are overestimated by as much as 12% with largest deviations for the smallest aspect ratio. Farther downstream, in the axisymmetric zone, velocities agree well with RANS simulations for all aspect ratios. Maximum deviations there are $\pm 2\%$.

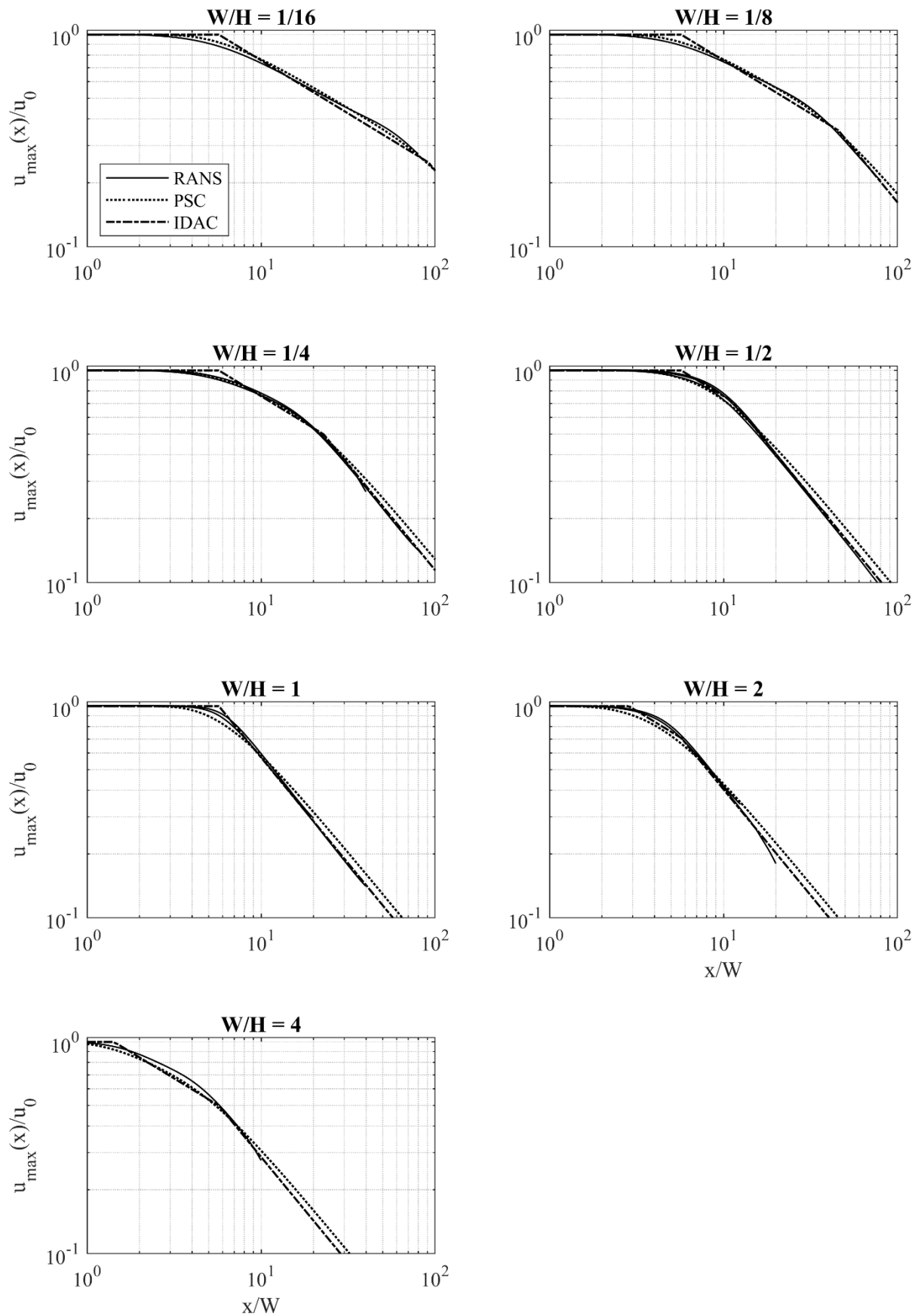


Figure 6: Evaluation of centerline velocity decay at the water surface ($z = 0$) from RANS simulations for W/H of 1/16, 1/8, 1/4, 1/2, 1, 2, and 4 in comparison with PSC and IDAC.

The longitudinal location of transition locations x_1 and x_2 between zones obtained from RANS simulations were evaluated in comparison to PSC and IDAC equations (Table 2). For the graphs obtained from RANS simulation and PSC, three tangents for the respective zones and approximated x_1 and x_2 from the intersections were applied. Locations of transitions using IDAC were calculated with eqs. (6) and (7). PSC predictions of transition locations of the core zone x_1 and the two-dimensional zone x_2 coincide with those obtained from RANS simulations for all aspect ratios. Similarly, IDAC predictions for x_1 for all aspect ratios and for x_2 for aspect ratios $W/H \geq 1/4$ coincide with RANS results. However, the transition between two-dimensional and axisymmetric zone for $W/H \leq 1/8$ is underestimated by IDAC with deviations of 23.4 % to 34.4 %. Note, while RANS and PSC are only visual estimates, the transition locations in IDAC can be calculated exactly.

Table 2: Transition locations x_1/W and x_2/W from RANS, PSC and IDAC according to eqs. (6) and (7)

W/H	RANS		PSC		IDAC	
	x_1/W	x_2/W	x_1/W	x_2/W	x_1/W	x_2/W
1/16	5.0	60	6.0	60	5.7	91.4
1/8	5.0	35	5.5	35	5.7	45.7
1/4	5.0	17	5.0	20	5.7	22.9
1/2	4.0	9.2	4.0	12	5.7	11.4
1	4.0	7.0	4.0	8.0	5.7	5.7
2	3.1	5.5	2.3	5.8	2.9	5.7
4	1.5	4.8	1.5	6.0	1.4	5.7

4.3 Jet half-length

Normalized jet half-lengths L_x/W (eq. ((1)) as predicted by PSC and IDAC were plotted against W/H of rectangular surface jets as a single comparative parameter to characterize longitudinal jet propagation together with half-lengths obtained from RANS simulations and previous studies (Figure 7). The boundary conditions for jets in the previous studies generally agree with those of the present study especially for homogeneous inlet flow conditions. PSC and IDAC predictions of jet half-lengths show small differences ($< 5\%$) for $1/4 \leq W/H \leq 4$, which includes the range typical for fishways. For $W/H < 1/4$ and $W/H \geq 10$ PSC predictions of L_x are up to 10 % larger than those of IDAC.

On a quantitative scale for aspect ratios up to 50, predictions of both models agree with results of RANS simulations and literature studies. Deviations may arise from differences in boundary conditions, e.g. measurements of Giger et al. (1991) were performed with an adjacent downstream channel bed which prevented vertical jet propagation in some cases and forced the jet to propagate farther downstream. For the most relevant range of aspect ratios ranging from 1/4 to 1, both models are in accordance with data from Gholamreza-Kashi et al. (2007), Rajaratnam and Humphries (1984) and Madnia and Bernal (1994) with maximum deviations of $\pm 15\%$. Half-length obtained from the present RANS simulations agree with maximum deviations of $\pm 5\%$.

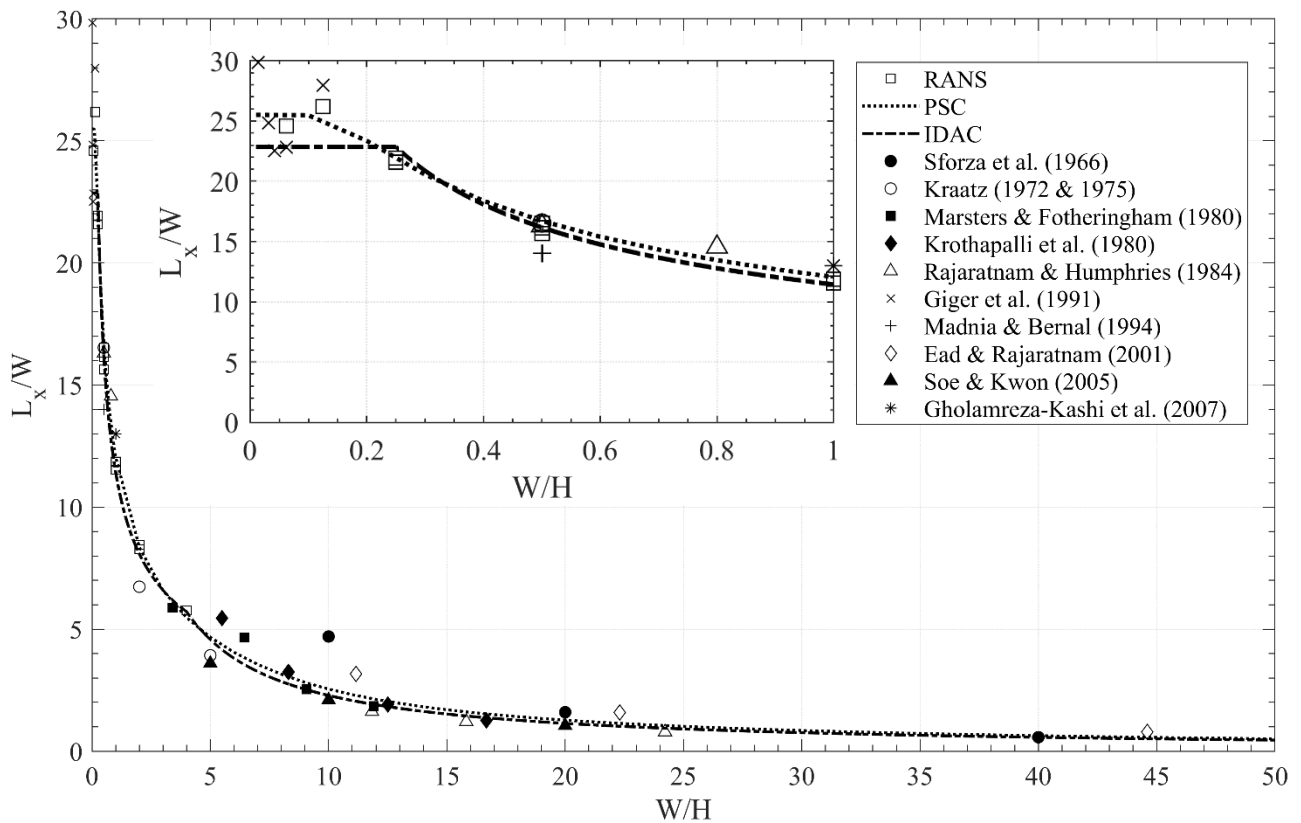


Figure 7: Comparison of predicted jet half-lengths of RANS, PSC, IDAC and experimental data from previous studies with detailed view for $0 \leq W/H \leq 1$ (inset). Values from previous studies were extracted from diagrams of centerline velocity decays. The solid symbols represent investigations on free jets.

4.4 Jet half-widths

The streamwise evolution of jet half-widths (eqs. ((2) and ((3)) was analyzed to quantify lateral and vertical propagation of rectangular surface jets. The spreading coefficient is determined as the slope of the half-width plotted against axial distance (eq. (13)). PSC predictions of half-width from eq. (4) were computed and compared against results obtained from RANS simulations for jets for $1/8 \leq W/H \leq 1/2$ (Figure 8). Half-widths are normalized with W and plotted against normalized streamwise distances x/W .

Both PSC and RANS simulations predict generally similar linear spreading of L_y along the minor axis. From Figure 8, the spreading coefficient of PSC for all aspect ratios converges to 0.10, which also fits well within the range of Demissie's (1980) results of $C = 0.097$; 0.095 and 0.104 for $W/H = 4$; 13 and 26, respectively. RANS results obtain spreading coefficients for $x > x_1$ of 0.083 for $W/H = 1/2$, 0.108 for $W/H = 1/4$ and 0.115 for $W/H = 1/8$. These results suggest that spreading coefficients depend on aspect ratio with jets with smaller W/H showing an increased spreading coefficient, although Demissie (1980) assumes that the spreading coefficient of free jets may be independent of the aspect ratio. Taking this into account, the spreading coefficient calculated for all RANS simulations considered here is determined to 0.117, independent of W/H . This is larger than the value of PSC, but is in the range of IDAC (not shown in the figure) with spreading coefficients of 0.128 and 0.095 measured by Kraatz (1975) for plane and round jets, respectively.

Curvilinear spreading along the major axis L_z is strongly influenced by the core zone and for $x < x_1$ the spreading rate is less than along the minor axis and gradually approaches the spreading rate determined for L_y in the axisymmetric zone. Transition locations x_2 for RANS simulations agree with those obtained visually given in Table 2 for jets with similar W/H . Based on Figure 8, the transition locations x_2 for PSC cannot be determined exactly as the lines approach each other asymptotically and x_2 occurs outside the displayed range.

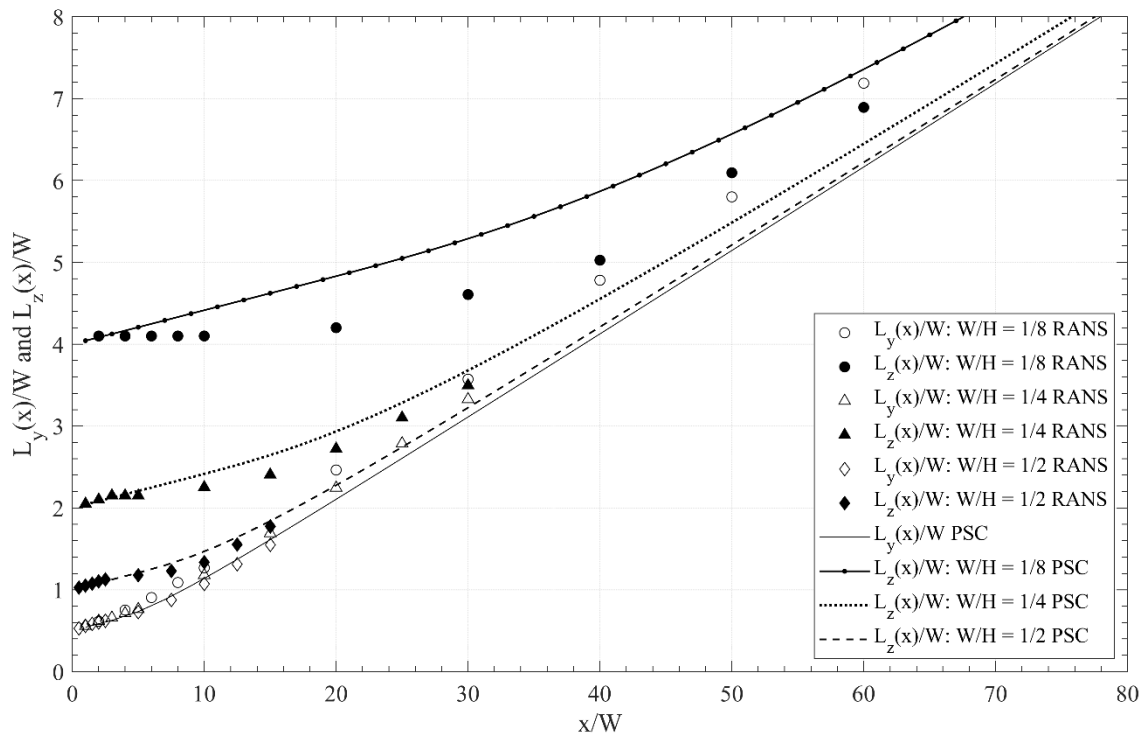


Figure 8: Jet half-widths $L_y(x)/W$ and $L_z(x)/W$ over x/W for aspect ratios 1/8, 1/4, and 1/2 from RANS and PSC. IDAC representation is omitted since it only provides values for spreading coefficients for plane and round jets.

5 Discussion

To verify the suitability of the existing analytical models for $W/H < 1$, a RANS model was used. The model was validated with experimental data for a surface jet with $W/H = 1$, where the core zone directly transitions to the axisymmetric zone. For aspect ratios other than 1, model validation data would have been desirable but are, to our knowledge, not available in literature. To increase trust in RANS simulation for surface jets that include a two-dimensional zone, an extensive comparison of L_x to literature values was performed. The agreement of the results suggests that the RANS model is suitable to correctly characterize three-dimensional surface jets. This is relevant in assessing fishway attraction flow where L_x may be located in either the two-dimensional or axisymmetric zone.

The results show that both analytical models are generally able to predict flow velocities and propagation of rectangular surface jets with good accuracy even when W/H of the fishway entrance slot changes in response to different tailwater levels. Maximum jet half-length inaccuracies of both models are as low as 5 % for aspect ratios $1/4 \leq W/H \leq 1$ common for fishway entrances. For smaller aspect ratios ($W/H < 1/4$) both analytical models show deviations as large as 15 % to RANS results and results from physical model investigations (Giger et al. 1991). IDAC gives more conservative results as predicted half-length are consistently lower (i.e., attraction flow propagation is underestimated) than results obtained from PSC. However, such small aspect ratios of entrance slots are rather unusual when constructing fishways.

Accurately locating transition locations (where two-dimensional velocity decay transitions into axisymmetric velocity decay) is crucial for accurate prediction of centerline velocities. Transition locations are well predicted by both analytical models so that either can be used to determine an optimal attraction flow propagation within the design discharge range. eqs. (5) or (8) – (11) indicate, in order to increase attraction flow propagation, it is a more efficient use of water to increase the outlet velocity u_0 of the fishway entrance because downstream location x increases as a quadratic with u_0 but linearly with orifice dimensions W or H .

The dimensions of the rectangular orifice can be optimized once the centerline velocity is fixed. However, maximum flow velocity must be less than the maximum swimming speed of target fish species. For vertical slots ($W/H < 1$) it is more effective to increase entrance width than water depth. Increase in length of the core zone contributes the most to

extending the attraction flow in the two-dimensional zone. The opposite holds for horizontal orifices, but these are atypical fishway geometries. For both cases velocities of the axisymmetric zone are independent of the orifice dimensions.

Both analytical models assume unbounded, quiescent tailwater basins, and ideal nozzles producing homogeneous flow conditions where flow velocities are equally distributed over the orifice section. In reality, boundary conditions at fishway entrances are more complex because of inhomogeneous approach flow to a vertical slot, presence of solid boundaries in the tailwater, and concurrent tailwater flows, e.g. due to releases from an adjacent hydropower plant. Thus, the derived models may be enhanced to address site-specific complexity by including adjustable coefficients (e.g., IDAC: inner diffusion angle, PSC: scale coefficient) or by adding constants to describe specific features (e.g. for propagation length (Mahl et al. 2021, Heneka et al. 2021)).

Both investigated models have differences in their analytical formulation which might be of importance during implementation of the equations in a design approach. Usage of PSC can be advantageous because it uses a single equation to describe downstream propagation while IDAC equations are formulated in multiple sections. In contrast, when using the approaches inversely to calculate entrance width for a targeted propagation length, IDAC may easily be inverted. No inverted analytical approach may be derived for PSC as it is formulated using products and sums of error functions.

6 Conclusions

The present study shows that existing and easy applicable approaches may be used to assess propagation of jets emergent from fishway entrances. Two analytical models for predicting jet propagation (Kraatz 1975, Demissie 1980), originally derived for rectangular free jets with orifice aspect ratios $W/H > 1$, where applied for surface jets with $W/H < 1$ and compared to RANS model results and values from previous studies. The results yield an accuracy of $< 5\%$ for $1/4 \leq W/H \leq 1$ compared to RANS and $\leq 15\%$ compared to literature results from surface jets. Since PSC and IDAC deliver reliable predictions of jet half-lengths L_x , either model may be equally used to assess attraction flow jets emergent from fishway entrances when boundary conditions are appropriate. However, for deviating boundary conditions which are likely to occur at actual sites in the form of, e.g. inlet or tailwater flow and geometry, further investigations are indicated (e.g. Mahl et al. 2021). In order to subsequently use the results of this study in a generic parametric approach for determining fishway attraction flow at dams with hydropower usage, constants to approximate the real and complex conditions were developed (Heneka et al. 2021).

Acknowledgements

The provision of experimental data from Dr. Soheil Gholamreza-Kashi is gratefully acknowledged. Useful reviews were provided by John Nestler of Fisheries and Environmental Services.

Author contributions (CRediT)

VW: Conceptualization, Data curation, Formal Analysis, Investigation, Methodology, Validation, Visualization, Writing – original draft. PH: Conceptualization, Investigation, Methodology, Validation, Supervision, Writing – review & editing. MH: Conceptualization, Supervision, Writing – review & editing. LB: Data curation, Investigation.

Notation

Name	Symbol	Unit
Spreading coefficient along the minor axis	C	-
Experimental spreading coefficient of the jet	c	-
Froude number	Fr	-
Orifice height or effective jet height	H	m
Turbulence intensity	I	-
Kinetic energy	k	m^2/s^2
Mixing length	L	m
Jet half-length	L_x	m

Jet half-width in lateral direction	L_y	m
Jet half-width in vertical direction	L_z	m
Reynolds number	Re	-
Hydraulic radius	R_{hy}	m
Velocity component in streamwise (x) direction	u	m/s
Outlet velocity	u_0	m/s
Maximum velocity at the centerline	$u_{max}(x)$	m/s
Slot width	W	m
Streamwise or longitudinal direction	x	m
Virtual origin	x_0	m
Transition location from the core to the two-dimensional zone	x_1	m
Transition location from the two-dimensional to the axisymmetric zone	x_2	m
Lateral direction	y	m
Vertical direction	z	m
Inner diffusion angle	α_i	°

References

- Castro-Santos, T.; Haro, A. (2010): Fish Guidance and Passage at Barriers. Fish locomotion: An eco-ethological perspective. Domenici, P.; Kapoor, B. G. (Ed.), pp. 62–89.
- Demissie, M. (1980): Diffusion of Three-Dimensional Slot Jets with Deep and Shallow Submergence. Dissertation. University of Illinois, Urbana-Champaign. Civil Engineering.
- Gholamreza-Kashi, S.; Martinuzzi, R. J.; Baddour, R. E. (2007): Mean Flow Field of a Nonbuoyant Rectangular Surface Jet. In *Journal of Hydraulic Engineering* 133 (2), pp. 234–239. DOI: 10.1061/(ASCE)0733-9429(2007)133:2(234).
- Giger, M.; Dracos, T.; Jirka, G. H. (1991): Entrainment and mixing in plane turbulent jets in shallow water. In *Journal of Hydraulic Research* 29 (5), pp. 615–642. DOI: 10.1080/00221689109498980.
- Heneka, P.; Zinkhahn, M.; Schütz, C.; Weichert, R. B. (2021): A Parametric Approach for Determining Fishway Attraction Flow at Hydropower Dams. In *Water* 13 (743). DOI: 10.3390/w13050743.
- Kopecki, I.; Schneider, M.; Tuhtan, J. A.; Schletterer, M. (2014): Assessment of attraction flow by the use of an agent based modelling technique in CASiMiR fish. 10th International Symposium on Ecohydraulics. Harby, Sundt (Ed.).
- Kraatz, W. (1975): Ausbreitungs- und Mischungsvorgänge in Strömungen. Dissertation. Technische Universität Dresden, Dresden, Germany.
- Krothapalli, A.; Baganoff, D.; Karamcheti, K. (1981): On the mixing of a rectangular jet. In *Journal of Fluid Mechanics* 107, pp. 201–220.
- Kümmel, Wolfgang (2004): Technische Strömungsmechanik. Theorie und Praxis. 2nd ed.: Vieweg + Teubner Verlag.
- Larinier, M. (1992): Implantation des passes à poissons. In *Bulletin Français de la Pêche et de la Pisciculture* (326–327), pp. 30–44. DOI: 10.1051/kmae:1992004.
- Madnia, K.; Bernal, L. P. (1994): Interaction of a Turbulent Round Jet with the Free Surface. In *Journal of Fluid Mechanics* 261, pp. 305–332. DOI: 10.1017/S0022112094000352.
- Mahl, L.; Heneka, P.; Henning, M.; Weichert, R. B. (2021): Numerical Study of Three-Dimensional Surface Jets Emerging from a Fishway Entrance Slot. In *Water* 13 (1079). DOI: 10.3390/w13081079.
- Marsters, G. F.; Fortheringham, J. (1980): The influence of aspect ratio on incompressible, turbulent flows from rectangular slots. In *Aeronautical Quarterly*, pp. 285–305.
- Menter, F. R.; Esch, T. (2001): Elements of industrial heat transfer predictions (16th Brazilian Congress of Mechanical Engineering, 20), pp. 117–127.
- Menter, F. R.; Kuntz, M.; Langtry, R. (2003): Ten Years of Industrial Experience with the SST Turbulence Model. In *Heat and Mass Transfer* 4.

- Patankar, S. V. (1980): *Numerical Heat Transfer and Fluid Flow*: CRC Press.
- Quinn, W. R. (1992): Turbulent Free Jet Flows Issuing from Sharp-Edged Rectangular Slots: The Influence of Slot Aspect Ratio. In *Experimental Thermal and Fluid Science* 5 (2), pp. 203–215.
- Quinn, W. R. (2006): Upstream nozzle shaping effects on near field flow in round turbulent free jets. In *European Journal of Mechanics B/Fluids* 25 (3), pp. 279–301. DOI: 10.1016/j.euromechflu.2005.10.002.
- Rajaratnam, N. (1976): *Turbulent jets*. Amsterdam, Oxford, New York: Elsevier Scientific Pub. Co (Developments in water science, 5).
- Rajaratnam, N.; Humphries, J. A. (1984): Turbulent non-bouyant surface jets. In *Journal of Hydraulic Research* 22 (2), pp. 103–115. DOI: 10.1080/00221688409499387.
- Reichardt, H. (1943): On a New Theory of free Turbulence. In *The Journal of the Royal Aeronautical Society* 47 (390), pp. 167–176. DOI: 10.1017/S0368393100106613.
- Rodi, W. (2017): Turbulence Modeling and Simulation in Hydraulics: A Historical Review. In *Journal of Hydraulic Engineering* 143 (5). DOI: 10.1061/(ASCE)HY.1943-7900.0001288.
- Seo, I. W.; Kwon, S. J. (2005): Experimental Investigation of Three-Dimensional Nonbouyant Rectangular Jets. In *Journal of Engineering Mechanics* 131 (7), pp. 733–746. DOI: 10.1061/(ASCE)0733-9399(2005)131:7(733).
- Sforza, P. M.; Steiger, M. H.; Trentacoste, N. (1966): Studies on Three-Dimensional Viscous Jets. In *AIAA Journal* 4 (5), pp. 800–806. DOI: 10.2514/3.3549.
- Tsuchiya, Y.; Horikoshi, C.; Sato, T. (1986): On the spread of rectangular jets. In *Experiments in Fluids* 4, pp. 197–204.
- Walker, D. T. (1997): On the origin of the 'surface current' in turbulent free-surface flows. In *Journal of Fluid Mechanics* (339), pp. 275–285. DOI: 10.1017/S0022112097005181.
- Weller, H. G.; Tabor, G.; Jasak, H.; Fureby, C. (1998): A tensorial approach to computational continuum mechanics using object-oriented techniques. In *Computers in Physics* 12 (6), pp. 620–631.
- Wiegel, R. L.; Mobarek, I.; Jen, Y. (1965): *Discharge of Warm Water Jets over Sloping Bottom*. Berkeley (USA).
- Williams, J. G.; Armstrong, G. S.; Katopodis, C.; Larinier, M.; Travade, F. (2012): Thinking like a fish: A key ingredient for development of effective fish passage facilities at river obstructions. In *River Research and Applications* 28 (4), pp. 407–417. DOI: 10.1002/rra.1551.